Andreev spectrum with high spin-orbit interactions: Revealing spin splitting and topologically protected crossings

A. Murani, A. Chepelianskii, S. Guéron, and H. Bouchiat
Laboratoire de Physique des Solides, CNRS, Université Paris-Sud, Université Paris Saclay, 91405 Orsay Cedex, France
(Received 15 November 2016; revised manuscript received 16 May 2017; published 9 October 2017)

In order to point out experimentally accessible signatures of spin-orbit interaction, we investigate numerically the Andreev spectrum of a multichannel mesoscopic quantum wire (N) with high spin-orbit interaction coupled to superconducting electrodes (S), contrasting topological and nontopological behaviors. In the nontopological case (square lattice with Rashba interactions), we find that the Kramers degeneracy of Andreev levels is lifted by a phase difference between the S reservoirs except at multiples of π, when the normal quantum wires can host several conduction channels. The level crossings at these points invariant by time-reversal symmetry are not lifted by disorder. Whereas the dc Josephson current is insensitive to these level crossings, the high-frequency admittance (susceptibility) at finite temperature reveals these level crossings and the lifting of their degeneracy at π by a small Zeeman field. We have also investigated the hexagonal lattice with intrinsic spin-orbit interaction in the range of parameters where it is a two-dimensional topological insulator with one-dimensional helical edges protected against disorder. Nontopological superconducting contacts can induce topological superconductivity in this system characterized by zero-energy level crossing of Andreev levels. Both Josephson current and finite-frequency admittance carry then very specific signatures at low temperature of this disorder-protected Andreev level crossing at π and zero energy.

DOI: 10.1103/PhysRevB.96.165415

I. INTRODUCTION

A number of intriguing phenomena have been predicted recently in which quantum wires made from materials with strong spin-orbit interaction (SOI) are used as weak links coupling two superconductors : spin-dependent supercurrents [1–3], supercurrents through edge states when the wire is made of a topological insulator [4–6], supercurrents at zero phase difference (ϕ_0 junctions) [7–12], and topologically protected zero-energy states [6,13]. Different materials have been used to experimentally explore some of these ideas: semiconducting nanowires (InAs or InSb) demonstrating ϕ_0 junctions [14] and probing Majorana physics [15–19], HgTe/HgCdTe or InAs/GaSb quantum-well heterostructures [20,21], BiSe flakes [22], and Bi nanowires [23,24], revealing ballistic supercurrent through helical edge states. The aim of this paper is to extract, from numerical simulations on two different types of lattices, observable signatures of spin-orbit interactions (SOI) which strongly modify the Andreev spectrum of these Josephson junctions.

We consider both the effects of the intrinsic atomic spin-orbit interactions that are specific to heavy atoms and are at the origin of the emergence of the spin-Hall insulator state for the hexagonal two-dimensional (2D) lattice [4,25], and the Rashba [26] SOI at 2D interfaces of semiconductors where inversion symmetry is broken.

By coupling the kinetic momentum to the electronic spin, Rashba SOI are known to break the spin degeneracy of electronic states in a quantum dot in the absence of any magnetic field. When the quantum wire is coupled to superconducting reservoirs, proximity-induced superconductivity leads to the formation of Andreev pairs which are the combination of time-reversed electron and hole states. In the absence of a phase difference between the superconducting (S) reservoirs, time-reversal symmetry and Kramers degeneracy impose that Andreev states built from time-reversed electron-hole states are degenerate in the presence of SOI. This is, however, no longer the case when the two superconducting reservoirs impose a finite phase difference ϕ on the boundary conditions of Andreev states. When this phase factor is different from a multiple of π, Andreev wave functions acquire imaginary components and Andreev levels lose their twofold degeneracy. The phase-dependent Andreev levels are therefore split in the presence of SOI. In Sec. II, we first discuss the conditions to induce spin-split Andreev states in the absence of any Zeeman field in a nontopological wire. This is illustrated by numerical results obtained by diagonalizing the Bogoliubov–de Gennes Hamiltonian of a quantum wire with a square lattice and Rashba spin-orbit interaction between superconducting electrodes. The effects of the geometry of the junction (length, number of channels, disorder, position of Fermi energy) are discussed. We then consider the Andreev spectrum of the 2D hexagonal lattice with next-nearest-neighbor spin-orbit couplings (equivalent to the implementation of atomic spin-orbit coupling at low energy) leading to a 2D topological insulator and a quantum spin-Hall state (Kane and Mele model [4]). As expected, we confirm, for wide enough samples, the presence of 1D ballistic Andreev edge states crossing each other at zero energy and robust against disorder. This zero-energy level crossing of Andreev levels is the signature of the topological character of induced superconductivity in this system. In Sec. III, we explore the consequences of these SOI-modified Andreev spectra on the Josephson current. For nontopological junctions, the Josephson current is only quantitatively modified. It is decreased in the absence of disorder, but is substantially increased in the diffusive regime. On the other hand, the phase dependence of the Josephson current is strongly modified by SOI in the case of the hexagonal lattice in the topological quantum spin-Hall regime with the emergence of a sharp discontinuity at π. This sawtooth shape is characteristic of 1D ballistic transport. The resilience to disorder and imperfect transmission at the NS interface of this sharp current phase relation in the wire reveals the topological

 ©2017 American Physical Society

protection. In Sec. IV, we show how the main features of the Andreev spectra discussed in Sec. II are best revealed by the phase dependence of the high-frequency admittance $Y = i\omega\chi$. We focus on the contribution that is proportional to the sum of i_n^2, the square of the single-level currents, in an energy window whose width is determined by temperature. This quantity is very sensitive to level anticrossings ($i_n^2 = 0$) or crossings (i_n^2 stays finite) in the Andreev spectrum. A very small Zeeman field breaks level degeneracy at 0 and π, yielding discontinuities in these single-level currents and consequently sharp dips in the dissipative response χ''.

The topological case is characterized by protected level crossings at zero energy and can be clearly identified in experiments measuring this dissipative response at very low temperature. χ'' is expected to exhibit a sharp peak at π, which increases at low temperature. This peak does not exist in the nontopological case, where instead dissipation is exponentially damped at low temperature and goes to zero at π. This result demonstrates the power of high-frequency experiments to probe the protection from disorder of Andreev edge states in a topological insulator.

II. ANDREEV SPECTRUM WITH SPIN-ORBIT INTERACTION

A. Square lattice with Rashba spin-orbit interaction

We first consider the case of a wire described by a tight-binding model on a 2D square lattice. We implement the Bogoliubov–de Gennes Hamiltonian described by the four blocks matrix,

$$\mathcal{H} = \begin{pmatrix} H - E_F & \Delta \\ \Delta^\dagger & E_F - H^* \end{pmatrix}. \tag{1}$$

The BCS matrix Δ couples electron and hole states of opposite spin, exclusively in the S part, and imposes the phase difference ϕ between the two superconducting reservoirs,

$$\boldsymbol{\Delta} = \boldsymbol{\Delta}_{is,i's'} = \exp(i\phi/2)\begin{pmatrix} 0 & -1 \\ 1 & 0 \end{pmatrix}. \tag{2}$$

H and $-H^*$ are $N \times N$ matrices that describe, respectively, the electron- and holelike spin-dependent wave functions of the hybrid NS wire with Rashba spin-orbit interaction [26],

$$H = \sum_{s,s'} \sum_{i=1}^{N} \epsilon_i(|i,s\rangle\langle i,s| + |i,s'\rangle\langle i,s'|) + \sum_{i\neq j} t_{ij}|i,s\rangle\langle j,s| + i\lambda_{ij}(\vec{e_z} \times \vec{u_{ij}})\vec{\boldsymbol{\sigma}}|i,s\rangle\langle j,s'| + \text{c.c.} \tag{3}$$

The vector $\vec{u_{ij}}$ connects the nearest-neighbor sites i and j, $\vec{e_z}$ is the unitary vector perpendicular to the plane of the sample, and $\vec{\boldsymbol{\sigma}}$ is the vector of Pauli matrices $\sigma_{x,y,z}$. The wire has $\mathrm{N} = N^N + N^S = N_x \times N_y$ sites on a square lattice of period a, with a normal part of $N^N = N_x^N \times N_y$ sites in contact on both sides with superconducting regions of length $N_x^S/2$, ($N^S = N_x^S \times N_y$ sites). The on-site random energies ϵ_i of zero average and variance W_d^2 describe the disorder in the wire. The hopping and spin-dependent coupling matrix elements $t_{ij} = t$ and $\lambda_{ij} = \lambda$ are restricted to the nearest neighbors. We have included the possibility to model imperfect transmission at the NS interface by taking reduced couplings $t_{ij}^{NS} < t$ along the NS interfaces. We have chosen the amplitude of the superconducting gap $\Delta = t/4$ and the number of superconducting sites larger than 30, such that the S coherence length $\xi_s = 2ta/\Delta \ll N_x^S$ in order to avoid any reduction of the superconducting correlations in the S region [27] (inverse proximity effect). We have checked that increasing the number of S sites does not change the spectrum of Andreev states below the superconducting gap. The number of transverse channels and the amplitude of the disorder correspond to the diffusive regime where the length $L = N_x^N a$ of the normal region is greater than the elastic mean free path l_e and shorter than the localization length $N_y l_e$. The length l_e is related to the amplitude of disorder by $l_e \simeq 15a(t/W_d)^2$ in 2D [28]. In the following, we will mostly focus on the long-junction limit where $L \gg \xi_s$. The amplitude of Rashba spin-orbit interactions is chosen to be larger than the superconducting gap and of the order of the Fermi energy. What we have in mind is typically surface states of bismuth where both Fermi and Rashba band splitting energies are of the order of 0.1 eV [29]. Beside Rashba spin-orbit interactions, intrinsic spin-orbit interactions are very strong in Bi. Depending on their orientation, some surfaces of Bi can also be topological and lead to quantum spin-Hall edge states [25]. This will be discussed in the next section.

For a purely 1D wire along the x axis, the Rashba spin-orbit coupling $H_R = \lambda p_x \sigma_y$ commutes with the 1D kinetic momentum. The spin components of the eigenstates are therefore polarized along the y axis. Their spatial components are Bloch waves whose wave vector is shifted by $\pm k_{SO} = 2m_{eff}\lambda/\hbar^2$ depending on the spin direction. In a finite-width wire, transverse channels corresponding to different k_y are coupled through the Rashba Hamiltonian $H_{R\perp} = \lambda p_y \sigma_x$. The eigenstates whose energy is close to the crossing points between these different channels display a spatially dependent spin texture and acquire different velocities along the x axis, as shown in [30,31] and Fig. 1. This distortion of the normal-state spectrum by SOI strongly affects the Andreev spectra in the long-junction limit.

In Fig. 1, we compare the Andreev spectra for a 1D wire with $N_y = 1$ and $N_y = 2$ transverse sites. In the case $N_y = 1$ [Fig. 1 (left)], the Andreev spectrum remains spin degenerate in the presence of spin-orbit interaction.

The situation is different for $N_y \geqslant 2$. The broken degeneracy of Andreev states at phases between 0 and π, observed in the Andreev spectrum of multichannel wires, results from the combination of electron and hole wave functions originating from different transverse channels coupled through Rashba SOI. When the chemical potential sits close to the bottom of the upper-energy spin-split subbands, as shown in [3,7] and Fig. 1, the Andreev states split into two families, corresponding to reversed spin states which have different velocities v^+ and v^- along the x axis. As shown in Fig. 1 (right), the eigenenergies of these states cross at 0 and π, as expected from time-reversal symmetry. In the long-junction limit, the phase dependence of Andreev states is determined by the Fermi velocity, and their spin degeneracy is therefore lifted for phase values different from 0 and π by an energy $\delta\epsilon_S$ of the order of $\hbar\pi(|v^+| - |v^-|)/L$, which can reach 0.5 $\delta\epsilon$,

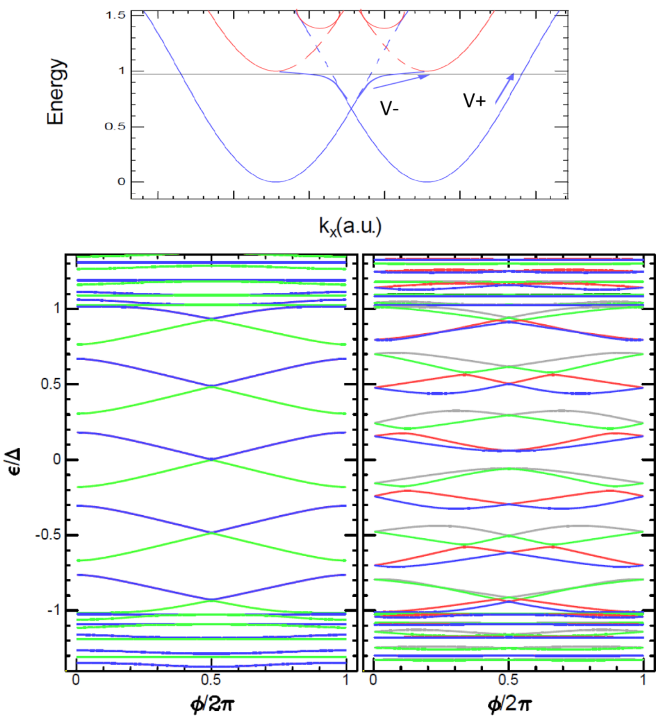

FIG. 1. Lifting of spin degeneracy of phase-dependent Andreev levels by SOI for ballistic wires ($L \ll l_e$) in the long-junction limit. Upper panel: Schematic tight-binding band structure of a two-channel ballistic wire in the presence of Rashba spin-orbit interactions. The transverse Rashba coupling opens a gap at the two band crossings leading to nonparabolic asymmetric dispersion relations. This distortion is at the origin of different velocities v^+ and v^- when the Fermi energy lies just below this gap. Lower panel, left: $N_y = 1$. Andreev spectrum is not modified by SOI. Lower panel, right: $N_y = 2$. The Fermi energy is taken at 1/4 of the tight-binding lower 1D band ($\epsilon_F = -t/2 = -2\Delta$), which corresponds to the bottom of the upper band. Note the breaking of spin degeneracy. (Parameters are $N_x = 50$, $\lambda = 3\Delta$. The number of S sites are, respectively, $N^S = 100 \times 1$ and $N^S = 100 \times 2$).

where $\delta\epsilon$ is the average level spacing. This mixing between transverse channels in a quantum wire induced by SOI was already discussed in a different context by Yokohama *et al.* in short junctions [10] as the condition to observe an anomalous Josephson current at $\phi = 0$ in the presence of a Zeeman field along the y axis (the so-called ϕ_0 junction behavior predicted by Buzdin and Reynoso [8,9] and only recently observed [14,24]).

When increasing the number of channels and on-site disorder W_d, one enters the diffusive regime. We still find a sizable splitting of Andreev levels of the order of the level spacing, with crossings at 0 and π at finite energy. Whereas in the ballistic regime SOI tends to reduce the phase dependence of the Andreev levels, we observe instead an increase of this phase dependence in the diffusive regime with a more pronounced harmonics content of the phase dependence of the eigenenergies; see Fig. 2. This splitting of Andreev levels is therefore a robust phenomenon in long SNS junctions with SOI and shows that the supercurrent in long SNS junctions is, in general, associated to a spin current of the order of $\mu_B(|v^+| - |v^-|)/L$.

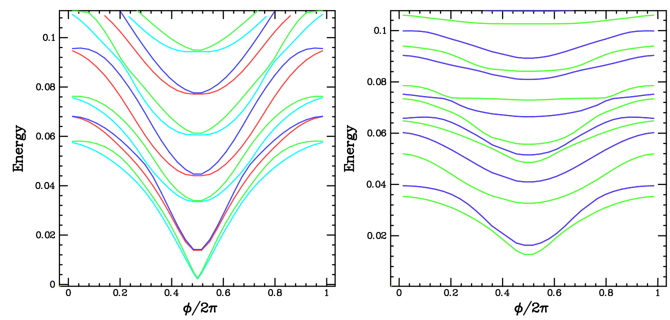

FIG. 2. Effect of SOI on the Andreev spectrum of a diffusive ribbon: $\lambda = 3\Delta$ (left), $\lambda = 0$ (right). Other parameters are $N_x^N = 50 \times 20$ normal sites with on-site disorder $W_d/t = 1$ corresponding to $L/l_e \simeq 2.5$, $\Delta = t/4$, $N^S = 30 \times 20$. Note the lifting of spin degeneracy as well as the larger and sharper phase dependence of Andreev levels in the presence of spin-orbit interactions.

B. Hexagonal lattice and quantum spin-Hall edge states

We now discuss the Andreev spectrum of graphenelike ribbons with $N^N = N_x \times N_y$ sites on an hexagonal lattice oriented along the armchair direction, in contact with two superconducting electrodes ($N^S = N_x^S \times N_y$ sites) on a square lattice (inset of Fig. 3). Following the model of Kane and Mele [4], the spin-orbit interaction is now implemented on the

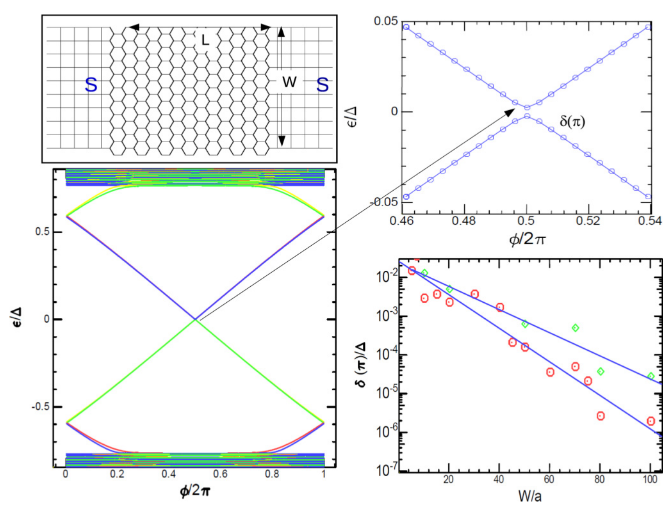

FIG. 3. Topological Andreev spectrum of a ribbon built with a hexagonal lattice with next-nearest-neighbor spin-orbit interactions. The ribbon is connected to nontopological superconducting electrodes with a square lattice. The Andreev spectrum is shown for $N_x = N_y = 20$ with on-site disorder $W_d = t$, corresponding to the diffusive regime in the absence of SOI. The amplitude of SOI is equal to the superconducting gap. Fermi energy is chosen to be $\epsilon_F = -0.33t$ and sits in the spin-orbit gap. The spectrum consists of two chiral Andreev levels corresponding to the two edges of the sample (short-junction limit). These states exhibit a linear phase dependence and cross at zero energy at phase π in the limit of very wide ribbons. Inset: exponential dependence of the residual gap at $\phi = \pi$ as a function of the sample width $W = N_y a$ for two different values of the superconducting gap $\Delta = 1$ (circles) and $\Delta = 0.5$ (diamonds).

next-nearest neighbors according to

$$H_{SO} = \sum_{s,s'=+,-} \sum_{i,j} + i\lambda_{ij}\sigma_{\mathbf{z}}|i,s\rangle\langle j,s'| + \text{c.c.}, \tag{4}$$

with $\lambda_{ij} = -\lambda_{ji} = \lambda$ couples next-nearest neighbors. At low energy, this model is equivalent to the implementation of an "intrinsic" spin-orbit interaction, which couples the real spin to the pseudospin and is opposite in sign for the two valleys of the Dirac spectrum. It leads to the opening of a spin-orbit gap at the Dirac points of the two valleys, and the formation of two counterpropagating, spin-polarized edge states characteristic of a 2D topological insulator. This model was initially proposed for graphene [4] whose intrinsic spin-orbit interaction is in the μ eV range. It was, however, shown that stronger spin-orbit interactions can be engineered by the deposition of a graphene layer on a crystalline transition-metal dichalcogenide (such as MoS_2 or WS_2) surface. The heavy Mo or W atoms induce spin-orbit interactions in the few-meV range in graphene [32]. The surface states on top of the (111) face of bismuth, which has hexagonal symmetry, have also been predicted to exhibit a 2D topological insulator state [25] with edge states protected from disorder. Signatures of these edge states were recently observed experimentally [24,33]. Moreover, very recently, bismuthene (a single layer of Bi with a hexagonal lattice) has been synthesized [34]. The following results obtained on the Andreev spectrum of a normal ribbon described by the Kane-Mele model coupled to nontopological superconducting reservoirs are relevant for all those systems. We believe it is important to simulate the realistic experimental situation where the ribbon made of a 2D topological insulator is connected on both edges to nontopological superconducting reservoirs, in contrast with the usual assumption [6] where the S electrodes connect only one edge of the sample. When the Fermi level lies in the spin-orbit gap, we find that the Andreev spectrum is identical to the spectrum of a single-channel ballistic wire with a pair of degenerate states crossing at zero energy for $\phi = \pi$. They correspond to the two helical edge states on the two sides of the wire that are not connected to superconducting electrodes (see Fig. 3).

In the presence of only intrinsic SOI and if the transmission along the SN interface is uniform, the two edge states are degenerate. As expected, this spectrum, shown in Fig. 3, is insensitive to disorder or reduced transmission at the NS interface, in contrast with the Andreev spectrum in the absence of intrinsic SOI. It does not depend on the transverse number of sites when the sample is much wider than the superconducting coherence length. The observed residual avoided crossing is due to the small coupling between the two edge states due to the finite width of the sample. In the range of parameters we considered where $\lambda \gg \Delta$, this coupling is mostly due to superconducting correlations. We indeed find that this residual gap at $\pi, \delta(\pi)$ decreases exponentially with the distance between the edges (i.e., the width of the sample), with a characteristic length given by the superconducting coherence length $\xi_S \simeq 10a$ for $\Delta = 1$ and $\xi_S \simeq 15a$ for $\Delta = 0.5$. This exponential decay of $\delta(\pi)$ with the width of the sample is a signature of the topological character of the Andreev spectrum and has to be contrasted with the $1/W$ dependence specific of nontopological spectra for systems in the diffusive regime

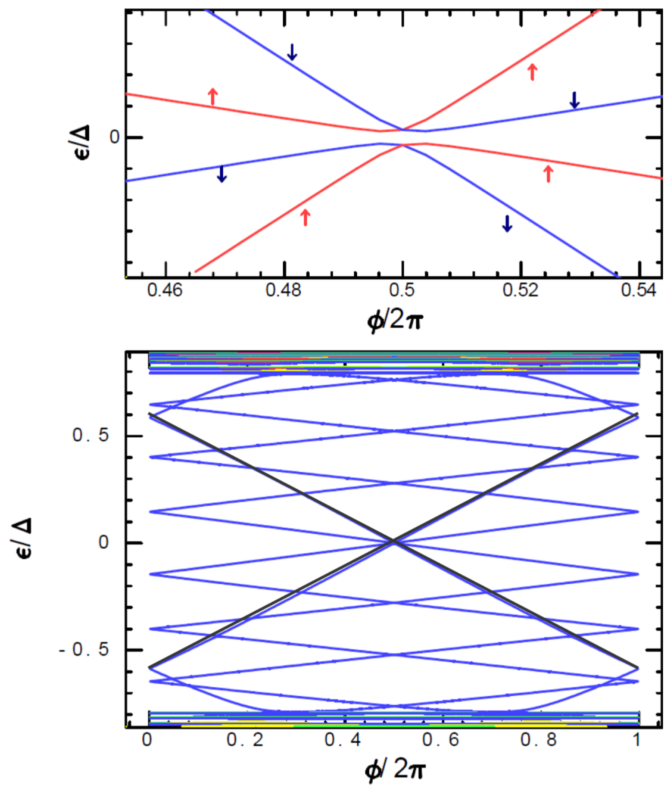

FIG. 4. Effect of S contact asymmetry on the topological Andreev spectrum. Bottom panel: Andreev level spectrum of a hexagonal lattice ribbon in the quantum spin-Hall phase with asymmetrical contacts on the edges, showing two distinct sets of Andreev levels corresponding to the two edges. Top panel: Expanded view of the spectrum close to zero energy showing unavoided level crossings between levels of opposite spin and avoided crossings between levels of the same spin corresponding to opposite edges. Parameters are $N_x = 10, N_y = 60, W_d = t/2 = 2\Delta, \lambda = 2\Delta, \epsilon_F = -\lambda/2, t_{SN}^{up} = 1, t_{SN}^{lw} = 0.1$.

(such as in Fig. 2). We have also investigated the situation where the transmission at the NS interface is different on the two edges of the ribbon. This is done by imposing $t_{SN}^{up} = 1$ at both NS interfaces along the upper half of the wire and $t_{SN}^{lw} < 1$ along the lower half. This asymmetry of the two edges gives rise to a lifting of the degeneracy between the Andreev levels. One clearly observes in Fig. 4 two distinct sets of spin-split Andreev levels corresponding to the two different edges. Both sets of Andreev levels exhibit a quasilinear phase dependence with crossings at zero and π characteristic of ballistic systems in good contact with superconducting electrodes. The spectrum corresponding to the well-coupled edge (in black) is identical to the spectrum shown in Fig. 3 with symmetrical contacts. In contrast, the set of Andreev levels associated to the weakly coupled edge (in blue) exhibits a smaller phase dependence corresponding to a ballistic SNS junction with an enhanced effective length of the order of $L + W/2$. This is because the wave function of this Andreev state along the bottom edge acquires a component along the bottom part of the NS interfaces with small values of t_{SN}. We also note the presence of small avoided crossings between states originating from different edges but with the same spin orientation. In contrast, states of opposite spins give rise, as expected, to unavoided crossings.

III. JOSEPHSON CURRENT AND CURRENT PHASE RELATION

At zero temperature, the Josephson current $I_J(\phi) = (2\pi/\phi_0)\partial E_J/\partial\phi$ is the derivative of the Josephson energy E_J, which is the sum of the phase-dependent energy levels below the Fermi energy. In the following, we compare the effect of SOI on the current phase relation $I_J(\phi)$ for nontopological Josephson junctions (square lattice with Rashba SOI) and topological ones (hexagonal lattice with intrinsic SOI).

A. Nontopological Josephson junctions with Rashba spin-orbit interaction

We first discuss the nontopological case corresponding to the square lattice with Rashba SOI whose Andreev spectrum is shown in Figs. 1 and 2. We have seen in the previous section that spin-orbit interaction strongly modifies the spectrum by lifting the spin degeneracy, leading to level crossings at phases multiple of π. This results in even phase-dependent contributions to the single-level currents, which are nonzero at 0 and π and opposite from one another for reversed spin states; see Fig. 5. The phase dependence of the total Josephson current is, however, not affected due to the compensation between these opposite current contributions of adjacent levels. This compensation does not occur for the spin current of the order of $\mu_B(|v^+| - |v^-|)/L$, which is, however, difficult to detect experimentally.

This is shown in Fig. 6 both for ballistic and diffusive wires in the long-junction limit whose Andreev spectra are shown in Figs. 2 and 3. One can see that the effect of spin-orbit interactions is opposite: the ballistic current is decreased whereas an increase of the amplitude of the Josephson current by a factor of two and a richer harmonics content are observed for the diffusive wire. The amplitude of the Josephson current with disorder is shown in the bottom panel of Fig. 6. In the ballistic regime corresponding to L smaller than the mean free path, the amplitude of the Josephson current is nearly independent of disorder and its phase dependence displays a strong anharmonicity. On the other hand, it decreases with disorder with a weaker harmonic content in the diffusive regime. A much weaker disorder dependence is observed in the presence of SO interactions. The crossover between the disorder-independent and disorder-dependent regimes takes place at larger values of disorder, which explains the larger amplitude and harmonics content of the current phase relation observed in the top panel of Fig. 6 with SO interactions. This enhanced resilience of Josephson current with disorder in the presence of SOI can be related to the phenomenon of antilocalization in quantum transport in the presence of spin-orbit interactions, inducing destructive interferences along time-reversed trajectories and leading to an increase of the conductance at low temperature [35]. This phenomenon has been shown to lead to a metal-insulator transition at 2D for a critical value of disorder with a metallic phase at low disorder that only exists if SOIs are present [36].

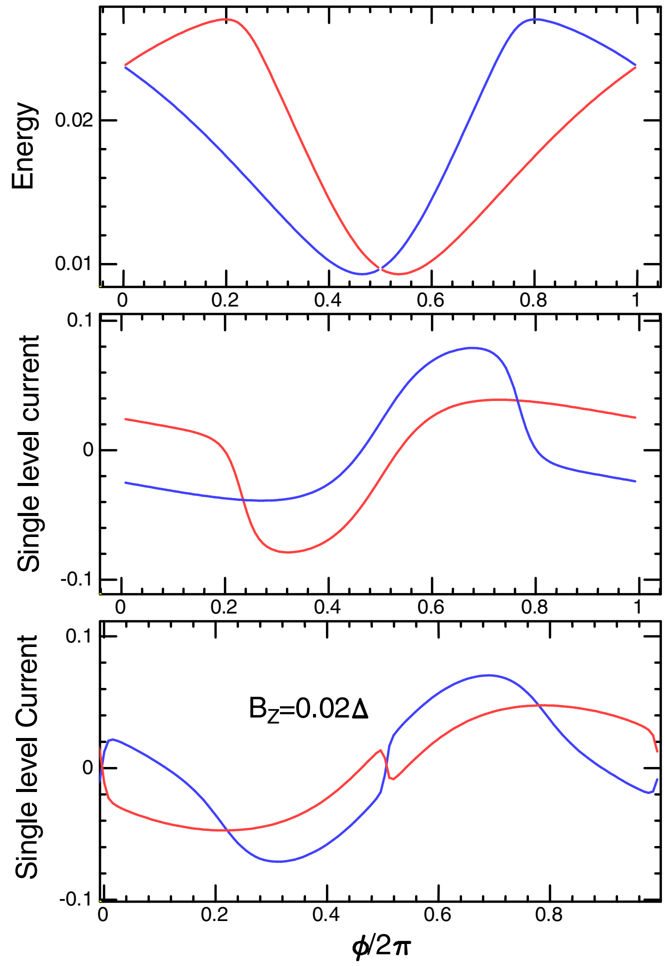

FIG. 5. From Andreev spectrum to Josephson current. Top panel: Phase dependence of the first two levels in the Andreev excitation spectrum of a square-lattice tight-binding wire, with Rashba SOI. Parameters are $N_x = 130$, $N_y = 4$, $W_d = 0.75t$, $\lambda = 2\Delta = t/2$. These two levels correspond to opposite spin states and cross each other at 0 and π. Middle panel: Currents carried by these levels; one can clearly identify, for these two single-level currents, a contribution which is an even function of phase, of opposite sign for the two levels. Bottom panel: Same quantity in the presence of a small Zeeman field perpendicular to the wire $E_Z = 0.02$ (in Δ units). Avoided crossings at 0 and π lead to discontinuities in the single-level currents, which become odd functions of phase.

Moreover, as expected and previously shown in other works [8–10], the combination of SOI with an in-plane Zeeman field B_Z leads to a ϕ_0 behavior.

B. Topological Josephson junctions

More spectacular behaviors are found when the normal part of the junction is built from the Kane and Mele topological insulator discussed in Sec. II B (hexagonal lattice with next-nearest-neighbor SOI) whose Andreev spectrum is shown in Fig. 3. As a result of the formation of topological edge states, the Josephson current is strongly modified by spin-orbit interactions and acquires a sawtooth shape with sharp discontinuities at odd multiples of π, which is characteristic of the Josephson current of a single-channel ballistic SNS junction.

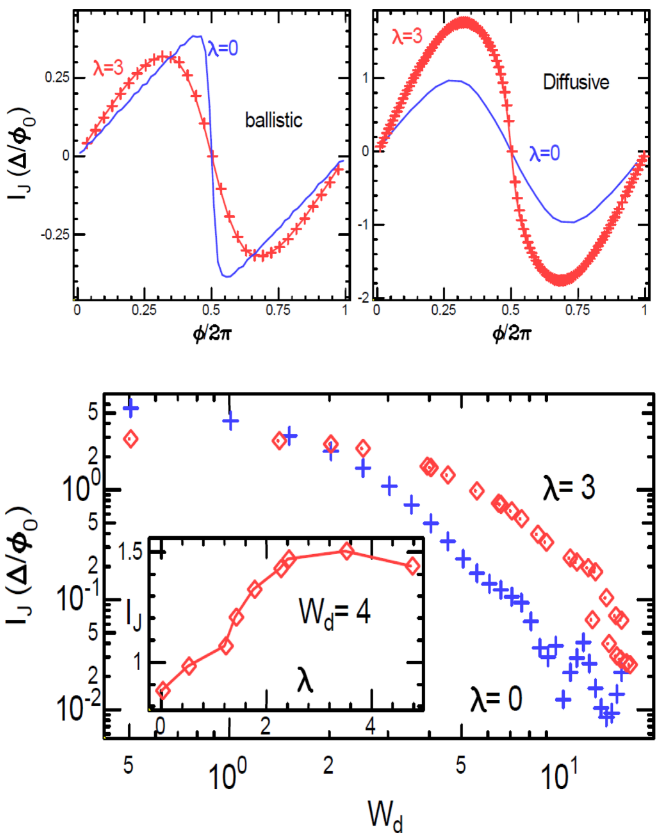

FIG. 6. Effect of spin-orbit interactions on the phase-dependent Josephson current for the square lattice with nearest-neighbor Rashba SOI interactions. Upper panel, left: Ballistic wire with $N_y = 2$ (same parameters as Fig. 1). Upper panel, right: Diffusive wire in the long-junction limit with the same parameters as Fig. 2. The amplitude and skewness of the phase-dependent Josephson current are decreased in the presence of SOI for the ballistic wire, whereas they are increased for the diffusive wire. Lower panel: Comparison of the disorder dependence of the Josephson current amplitude with and without Rashba spin-orbit interactions. One observes a weaker disorder dependence in the presence of spin-orbit interactions. The inset shows the increase of the Josephson current with λ up to $\lambda = 4 = t$ in the diffusive regime at $W_d = 4$.

The Josephson current is independent of the number of transverse channels and disorder. The sawtooth shape also resists to low-transmission NS interfaces with $T = (t_{SN}/t)^2 \ll 1$, in contrast with nontopological junctions as shown in Fig. 7. The amplitude of the sawtooth period which is proportional to the Thouless energy period is decreased for imperfect transmission at the NS interface, but the discontinuity at π is robust. Measuring this sawtooth current phase relation in *disordered* systems can therefore be considered as a signature of topological edge states protected against disorder. This was done recently in Bi nanowires [24]. Furthermore, topological crossings between Andreev states of opposite spin are expected to give rise to a 4π periodicity in the limit of decoupled edge states ($W \gg \xi$), which reflects the parity conservation within Andreev states [37]. This effect is, however, very difficult to detect experimentally because of unavoidable quasiparticle poisoning, leading to the conversion of an electron or hole spin-polarized state in the Andreev spectrum into a quasiparticle

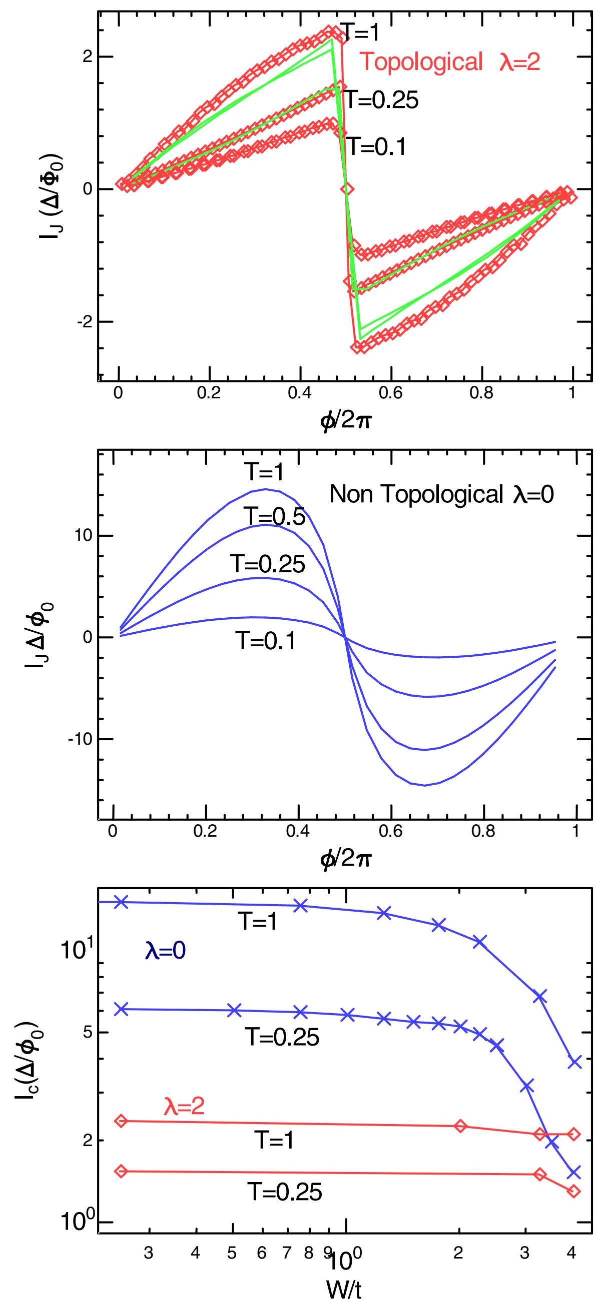

FIG. 7. Phase-dependent Josephson current for a topological junction compared to a nontopological one: hexagonal lattice with SOI $\lambda = 2\Delta$ and without SOI for different transmissions (uniform along the NS interface). Other parameters are $N_x = 10$ and $N_y = 60$. Upper panel: In the presence of SOI, the Josephson current exhibits a sawtooth shape with sharp discontinuities at odd multiples of π, which is characteristic of a 1D ballistic SNS junction. The amplitude of the sawtooth is decreased for imperfect transmission at the NS interface but the discontinuity at π is robust. The curves with diamond points correspond to a small disorder $W_d/t = 0.25$, whereas green solid lines correspond to larger values and a perfect transmission at the S/N interfaces, $W_d/t = 2$ and $W_d/t = 3$. Middle panel: The current phase relation (CPR) without SOI, for $W_d/t = 0.25$ for different NS interface transmissions T between 0.1 and 1. The CPR turns harmonic as τ decreases. Lower panel: Contrast of the disorder dependence of the amplitude of the Josephson current for different transmission coefficients for topological and nontopological junctions.

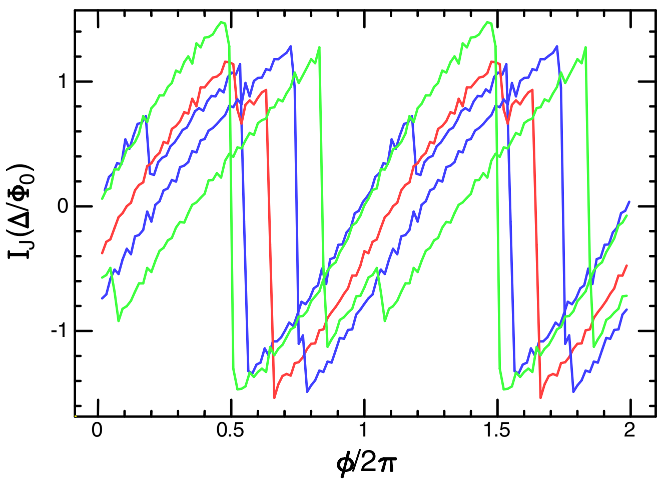

FIG. 8. ϕ_0 junction behavior in a topological wire with out-of-plane Zeeman field. The phase-dependent Josephson current in the Kane-Mele model with asymmetric NS coupling between the two edges is shown for different values of B_Z, going from 0 to 0.3 from top to bottom (in Δ units). Fermi energy is taken at $-t/4$ in the spin-orbit gap. Other parameters are similar to those in Fig. 4, $N_x = 20$, $N_y = 60$, $\lambda = 2\Delta$, $\epsilon_F = -\lambda/2$, $t_{SN}^{up} = 1$, $t_{SN}^{lw} = 0.1$.

above the superconducting gap [37,38]. We will discuss in the next section how high-frequency experiments instead can reveal this topological crossing at π.

When the transmissions of the contacts are different on the two edges, we find (see Fig. 8) that a Zeeman field gives rise to a ϕ_0 junction behavior. One observes a continuous phase shift of the Josephson relations together with abrupt discontinuities for certain values of B_Z. This behavior is related to the existence of spin-split phase-dependent states because of the asymmetry between the two edges, as seen in Fig. 4. It was also previously pointed out by Dolcini *et al.* [39] who also considered asymmetric edge states, considering different lengths for the two edges.

IV. NONADIABATIC FINITE-FREQUENCY RESPONSE

In this section, we show that the finite-frequency current susceptibility, which is the nonadiabatic linear current response to an ac phase bias, can be more sensitive to spin-orbit interactions than the dc Josephson current discussed above. As previously shown [40,41], this susceptibility can be investigated experimentally in an rf superconducting quantum interference device (SQUID) geometry where a hybrid NS ring is inductively coupled to a microwave cavity, generating a small ac flux superimposed on a dc Aharonov-Bohm flux. The induced shifts of the resonance frequency and quality factor yield, respectively, the nondissipative and dissipative components of this susceptibility $\chi(\omega)$. It is related to the admittance by $\chi(\omega) = i\omega Y(\omega)$ and can be computed from the eigenstates of the ring using a Kubo formalism [42],

$$\chi(\omega) = \frac{\partial I_J}{\partial \phi} - \sum_n i_n^2 \frac{\partial f_n}{\partial \epsilon_n} \frac{i\omega}{\gamma_D - i\omega} - \sum_{n,m\neq n} |J_{nm}|^2 \frac{f_n - f_m}{\epsilon_n - \epsilon_m} \frac{i\hbar\omega}{i(\epsilon_n - \epsilon_m) - i\hbar\omega + \hbar\gamma_{ND}}. \tag{5}$$

J_{nm} is the matrix element of the current operator between the Andreev eigenstates n and m of energies ϵ_n, and ϵ_m, f_n is the Fermi Dirac function. The first term is the zero-frequency susceptibility of the ring, which is the flux derivative of the Josephson current $\chi(0) = \partial I_J/\partial\phi$. The second and third terms, χ_D and χ_{ND}, only exist at finite frequency and describe the dynamic responses due, respectively, to the relaxation of the populations and to the transitions between the levels induced by microwave photon emission or absorption. The quantities γ_D and γ_{ND} are, respectively, the diagonal and nondiagonal relaxation rates of the system determined by its interaction with its thermodynamic environment. Both χ_D and χ_{ND} give rise to frequency-dependent dissipation described by their imaginary components. χ''_{ND} corresponds to microwave-induced resonant transitions in the Andreev spectrum and yields the spectroscopy of Andreev levels. χ''_{ND} has been explored experimentally by continuously sweeping the frequency of a microwave field injected in parallel to the field exiting the cavity at resonance (two-tone spectroscopy) [43] or by coupling the NS ring to a broadband Josephson spectrometer [44,45]. In the following, we focus on the less investigated contribution χ''_D, which yields the largest contribution at low frequency (compared to the induced gap). We note that this contribution, proportional to the single-level current squared, is specific to phase-dependent spectra (such as in Aharonov-Bohm rings) [46] and is ignored in most derivations of the Kubo formula,

$$\chi''_D = -\frac{\omega\tau_{in}}{(1+\omega^2\tau_{in}^2)} \sum_n i_n^2 \frac{\partial f_n}{\partial \epsilon_n} \tag{6}$$

(with $\tau_{in} = \gamma_D^{-1}$). This quantity has a very peculiar phase dependence: it displays a singularity at π in a diffusive wire with a continuous Andreev spectrum, due to the closing of the minigap. It was calculated by Lempitsky in 1983 [47–49], but only directly measured recently by Dassonneville *et al.* [41].

A. High temperature: Revealing crossings in the finite-energy Andreev spectrum

When the temperature is large compared to ϵ_n, $\frac{\partial f_n}{\partial \epsilon_n}$ can be approximated by $1/k_B T$ in Eq. (6). As a result, when $T \geqslant \Delta$, χ''_D is proportional to $S_2 = \langle \sum_n i_n^2 \rangle$ with the average running over the whole spectrum [40,48]. In the presence of SOI, the Andreev levels cross at 0 and π. As a result, the single-level quantities i_n and i_n^2 are finite at 0 and π, as well as the sum S_2. The resulting phase dependence of χ''_D is very different from its characteristic dependence without SOI, which is zero at multiples of π (because of disorder-induced avoided crossings between spin-degenerate Andreev levels). Moreover, this phase dependence with SOI is extremely sensitive to a Zeeman field perpendicular to the wires which couples levels of opposite in-plane spins and opens small gaps at $\phi = n\pi$. As shown in Fig. 5, Zeeman-induced avoided crossings give rise to discontinuities in $i_n(\phi)$ and sharp peaks in i_n^2 and S_2. This leads to a phase dependence of χ''_D which exhibits sharp singularities at 0 and π. This extreme sensitivity of χ''_D to a small perpendicular Zeeman field carries the signature of the spin-orbit spin splitting of Andreev levels, as shown in Fig. 9, comparing the phase dependence of χ''_D with and without SOI. This behavior is expected to be observed in any Andreev level

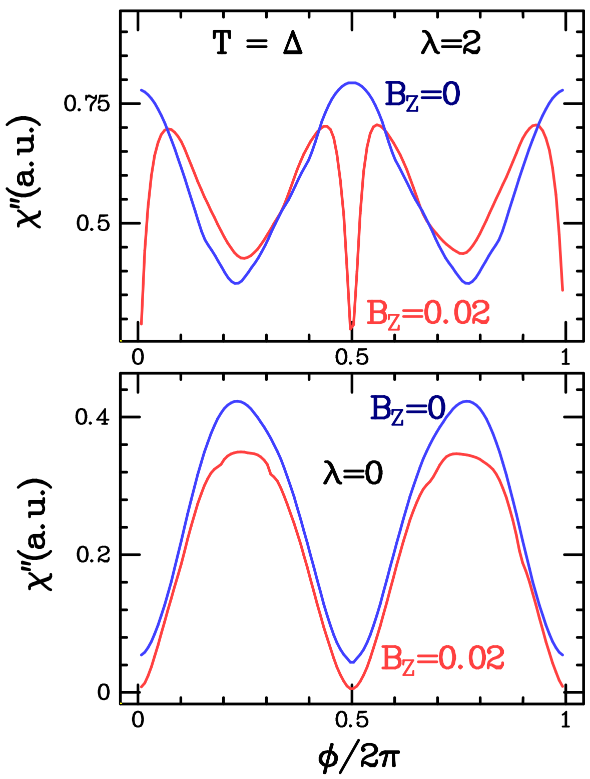

FIG. 9. Phase dependence of χ_D'' for the square lattice (nontopological regime) at a temperature equal to the superconducting gap. As explained in the text, this quantity is close to the squared single-level current, averaged over the whole spectrum. It is nearly π periodic in the absence of spin-orbit interactions (lower panel) and insensitive to a small Zeeman field (blue curve $B_Z = 0$, red curve $B_Z = 0.02$). The same quantities are shown in the presence of spin-orbit interactions $\lambda = 2\Delta$ in the upper panel. Spin splitting and crossings of the energy levels at $\phi = 0$ and π give rise to a very different behavior with broad maxima at 0 and π reflecting levels crossings, and sharp dips in a Zeeman field. Numerical simulations correspond to $N_x = 100$ and $N_y = 4$ with a square lattice. The amplitude of disorder is $W_d = 3\Delta$, yielding $L/l_e = 3.7$.

spectrum with spin-split Andreev levels and therefore does not yield information on the topological nature of the Andreev spectrum.

B. Low temperature: Revealing topological crossings at zero energy

We have so far discussed the phase dependence of χ_D'' at temperatures of the order or larger than the superconducting gap. In the low-temperature limit, the derivative of the Fermi function in expression (6) selects the very low-energy contribution (below $k_B T$) of the Andreev levels. For a nontopological spectrum (see Fig. 10), χ_D'' vanishes if the temperature is smaller than the energy gap at π separating electrons and hole states. This sensitivity to the existence or absence of energy levels at zero energy can be exploited to reveal the presence of topological crossings at zero energy, as we discuss below.

We move to the case of the Kane and Mele topological insulator in the presence of protected crossings at zero energy yielding nonzero single-level current at π. When the

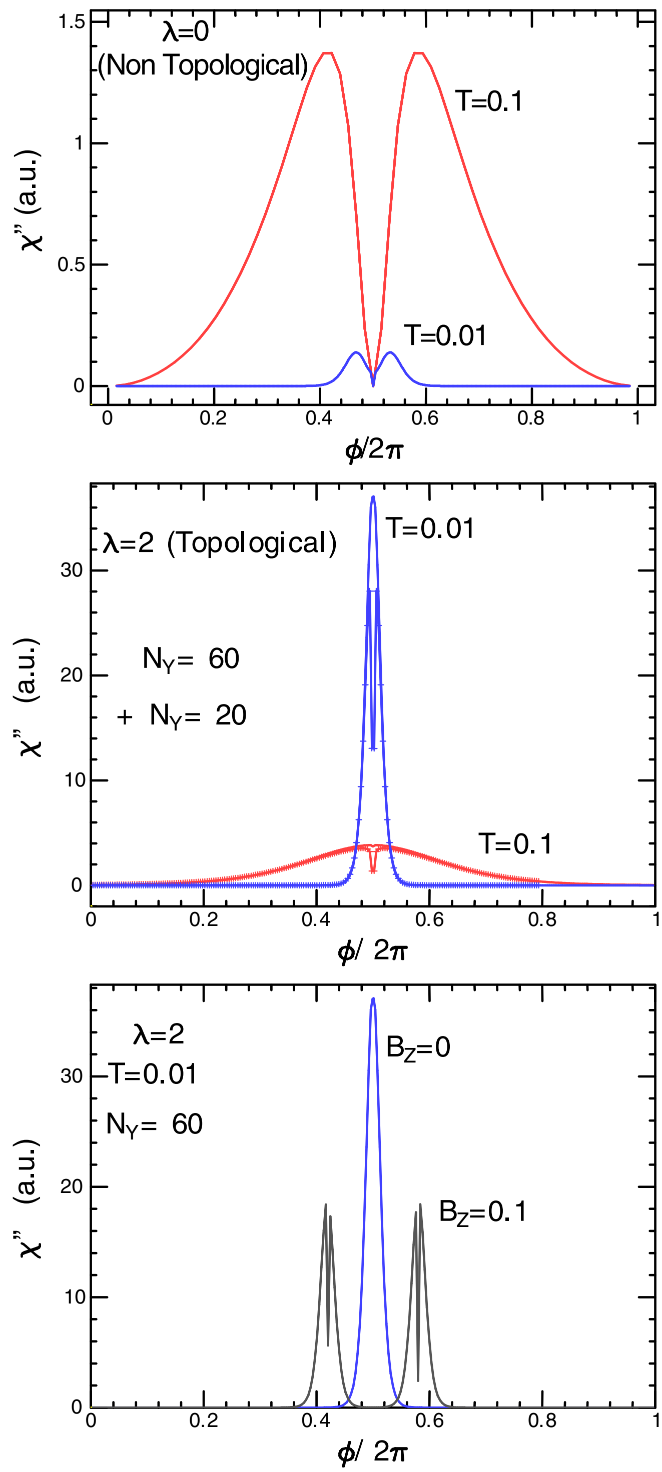

FIG. 10. Phase dependence of χ_D'' computed for the hexagonal lattice in the nontopological (no SOI, upper panel) and topological regimes (with SOI $\lambda = 2\Delta$, lower panels), at temperatures equal to 0.01Δ (blue) and 0.1Δ (red). Other parameters are $N_x = 10$ and $N_y = 60$. In the topological regime, we also show data for $N_y = 20$ (crosses). The peak at π carries the signature of the disorder-protected level crossing in the spectrum and is very sensitive to the presence of the coupling between the edges when the width of the sample is of the order of the superconducting coherence length. The lowest panel illustrates the effect of a Zeeman field which splits the zero-energy level crossing into two crossings that are symmetric around π.

temperature is much smaller than the superconducting gap, $\chi''_D(\phi)$ does not go to zero and exhibits a sharp peak at π, as shown in Fig. 10. However, because of the finite width of the wire, the two edge states are coupled at the NS interface. This coupling leads to an exponentially small avoided crossing of the levels at π and to a sharp and narrow dip of $\chi''_D(\phi)$ within the peak at π. This dip observed for $N_y = 20$ fades out when the wire is much wider than the superconducting coherence length. When this coupling between edge states is negligible, $\chi''(\pi)$ diverges at low temperature as $1/T$, like the derivative of the Fermi function at zero energy. In contrast, the split peak in the nontopological case has an amplitude which varies like $\partial f/\partial\epsilon = 1/4k_BTch^2(\delta/2k_BT)$, where δ is the level spacing around π. It is therefore exponentially depressed at low temperature compared to δ. In this comparison, shown in Fig. 10, we neglect the temperature and phase dependence of the phenomenological parameter $\tau_{\rm in}$, which should also be considered. $\tau_{\rm in}$ was experimentally determined for diffusive SNS junctions from the measurement of the frequency dependence of χ_D and found to be in the ns range at 1 K. We expect its value to be enhanced due to topological protection in quantum spin-Hall systems and to be limited by the coupling between the edges and quasiparticle poisoning. This signature of a topological crossing as a sharp peak in χ''_D at $\phi = \pi$ is strongly related, through the fluctuation dissipation theorem, to the Josephson current thermal noise $S(\omega) = 2k_BT\chi''_D(\omega)/\pi\omega$ as initially derived for atomic contacts [50] and, more recently, in [6] in the context of quantum spin-Hall insulators-based Josephson junctions. We also find that this peak of dissipation at π is split by a Zeeman field perpendicular to the plane (i.e., along the SO axis in the Kane-Mele model). We expect instead, in the nontopological case, peaks of dissipation to show up at very low temperature only if a Zeeman field is applied perpendicularly to the Rashba SO field.

This dissipation peak at π in the nonadiabatic linear response function and its splitting in a small Zeeman field also presents strong similarities with the predictions of [51] in the normal state. It should provide a unique signature of the nature of the level crossing at zero energy and constitutes therefore a stringent check of the topological nature of the Andreev spectrum. This is different from the proposals of Refs. [52–54] focused on the contribution of the nondiagonal elements, χ''_{ND}, coupling Andreev states to the continuum above the gap. Those transitions involve frequencies of the order of the superconducting gap or Thouless energy for long junctions, whereas we have discussed smaller frequencies, of the order of $1/\tau_{\rm in}$.

V. CONCLUSION

From the analysis of the phase-dependent Andreev spectrum of SNS junctions, we have extracted several observable signatures of large spin-orbit interactions. The phase dependence of the dc Josephson current is very sensitive to the formation of disorder-protected topological edge states. On the other hand, measurements of the current response to a small ac phase bias are very sensitive to the spin splitting of the Andreev states. At temperatures of the order of the superconducting gap, such measurements should reveal crossings between Andreev levels at multiples of π and their sensitivity to small Zeeman fields both in topological and nontopological junctions. By contrast, at very low temperature, these finite-frequency experiments can be used to reveal the presence of topological crossings at zero energy. These experiments can be conducted very close to thermodynamic equilibrium, in contrast to the switching current measurements proposed in [54]. They also allow an independent control of the amplitude and frequency excitation. This is not the case in ac Josephson effect measurements from which it is very difficult to disentangle topological effects from out-of-equilibrium Zener tunneling effects.

ACKNOWLEDGMENTS

We acknowledge R. Aguado, C. Bena, B. Dassonneville, R. Deblock, M. Ferrier, M. Houzet, J. Meyer, H. Pothier, P. Simon, and M. Trif for fruitful discussions as well as V. Croquette for great help in making a user-friendly interface for the program written by A. Chepelianskii. We have benefited from financial support of Grants No. MASH ANR-12-BS04-0016 and No. DIRACFORMAG ANR-14-CE3L-003 of the French Agency of Research.

[1] Nikolai M. Chtchelkatchev and Yu. V. Nazarov, Phys. Rev. Lett. **90**, 226806 (2003).
[2] B. Béri, J. H. Bardarson, and C. W. J. Beenakker, Phys. Rev. B **77**, 045311 (2008).
[3] Andres A. Reynoso, Gonzalo Usaj, C. A. Balseiro, D. Feinberg, and M. Avignon, Phys. Rev. B **86**, 214519 (2012).
[4] C. L. Kane and E. J. Mele, Phys. Rev. Lett. **95**, 146802 (2005); **95**, 226801 (2005).
[5] L. Fu and C. L. Kane, Phys. Rev. Lett. **100**, 096407 (2008).
[6] L. Fu and C. L. Kane, Phys. Rev. B **79**, 161408 (2009).
[7] I. V. Krive, L. Y. Gorelik, R. I. Shekhter, and M. Jonson, J. Low Temp. Phys. **30**, 398 (2004).
[8] A. Buzdin, Phys. Rev. Lett. **101**, 107005 (2008).
[9] A. A. Reynoso, G. Usaj, C. A. Balseiro, D. Feinberg, and M. Avignon, Phys. Rev. Lett. **101**, 107001 (2008).
[10] T. Yokoyama, M. Eto, and Y. V. Nazarov, Phys. Rev. B **89**, 195407 (2014).
[11] Konstantin N. Nesterov, Manuel Houzet, and Julia S. Meyer, Phys. Rev. B **93**, 174502 (2016).
[12] G. Campagnano, P. Lucignano, D. Giuliano, and A. Tagliacozzo, J. Phys.: Condens. Matter **27**, 205301 (2015).
[13] J. D. Sau, R. M. Lutchyn, S. Tewari, and S. DasSarma, Phys. Rev. Lett. **104**, 040502 (2010); M. Cheng and R. M. Lutchyn, Phys. Rev. B **86**, 134522 (2012).
[14] D. B. Szombati, S. Nadj-Perge, D. Car, S. R. Plissard, E. P. A. M. Bakkers, and L. P. Kouwenhoven, Nat. Phys. **12**, 568 (2016).

[15] V. Mourik, K. Zuo, S. M. Frolov, S. R. Plissard, E. P. A. M. Bakkers, and L. P. Kouwenhoven, Science **336**, 1003 (2012).
[16] M. T. Deng, C. L. Yu, G. Y. Huang, M. Larsson, P. Caroff, and H. Q. Xu, Nano Lett. **12**, 6114 (2012).
[17] A. D. K. Finck, D. J. Van Harlingen, P. K. Mohseni, K. Jung, and X. Li, Phys. Rev. Lett. **110**, 126406 (2013).
[18] H. Zhang, Onder Gul, S. Conesa-Boj, K. Zuo, V. Mourik, F. K. de Vries, J. van Veen, D. J. van Woerkom, M. P. Nowak, M. Wimmer, D. Car, S. Plissard, E. P. A. M. Bakkers, M. Quintero-Pérez, S. Goswami, K. Watanabe, T. Taniguchi, and L. P. Kouwenhoven, Nat. Commun. **8**, 16025 (2017).
[19] S. M. Albrecht, A. P. Higginbotham, M. Madsen, F. Kuemmeth, T. S. Jespersen, J. Nygard, P. Krogstrup, and C. M. Marcus, Nature (London) **531**, 206 (2016).
[20] S. Hart, H. Ren, T. Wagner, P. Leubner, M. Malbauer, C. Brune, H. Buhmann, L. W. Molenkamp, and A. Yacoby, Nat. Phys. **10**, 638 (2014).
[21] V. S. Pribiag, A. J. A. Beukman, F. Qu, M. C. Cassidy, C. Charpentier, W. Wegscheider, and L. P. Kouwenhoven, Nat. Nano **10**, 593 (2015).
[22] J. Wiedenmann, E. Bocquillon, R. S. Deacon, S. Hartinger, O. Herrmann, T. M. Klapwijk, L. Maier, C. Ames, C. Brüne, C. Gould, A. Oiwa, K. Ishibashi, S. Tarucha, H. Buhmann, and L. W. Molenkamp, Nat. Commun. **7**, 10303 (2016).
[23] C. Li, A. Kasumov, Anil Murani, Shamashis Sengupta, F. Fortuna, K. Napolskii, D. Koshkodaev, G. Tsirlina, Y. Kasumov, I. Khodos, R. Deblock, M. Ferrier, S. Guéron, and H. Bouchiat, Phys. Rev. B **90**, 245427 (2014).
[24] A. Murani, Alik Kasumov, Shamashis Sengupta, Yu. A. Kasumov, V. T. Volkov, I. I. Khodos, F. Brisset, R. Delagrange, Alexei Chepelianskii, Richard Deblock, Helene Bouchiat, and Sophie Guéron, Nat. Commun. **8**, 15941 (2017).
[25] S. Murakami, Phys. Rev. Lett. **97**, 236805 (2006).
[26] Y. A. Bychkov and E. I. Rashba, Pis'ma Zh. Eksp. Teor. Fiz. **39**, 66 (1984) [Sov. Phys. JETP Lett. **39**, 78 (1984)].
[27] M. Buttiker and T. M. Klapwijk, Phys. Rev. B **33**, 5114 (1986).
[28] G. Montambaux, H. Bouchiat, D. Sigeti, and R. Friesner, Phys. Rev. B **42**, 7647 (1990).
[29] P. Hoffman, Prog. Surf. Sci. **81**, 191 (2006).
[30] M. Governale and U. Zulicke, Phys. Rev. B **66**, 073311 (2002).
[31] T. Meng, Jelena Klinovaja, and D. Loss, Phys. Rev. B **89**, 205133 (2014); D. Bercioux and P. Lucignano, Rep. Prog. Phys. **78**, 106001 (2015).
[32] Z. Wang, D.-K. Ki, J. Y. Khoo, D. Mauro, H. Berger, L. S. Levitov, and A. F. Morpurgo, Phys. Rev. X **6**, 041020 (2016).
[33] Ilya K. Drozdov, A. Alexandradinata, Sangjun Jeon, Stevan Nadj-Perge, Huiwen Ji, R. J. Cava, B. A. Bernevig, and A. Yazdani, Nat. Phys. **10**, 664 (2014).
[34] F. Reis, G. Li, L. Dudy, M. Bauernfeind, S. Glass, W. Hanke, R. Thomale, J. Schäfer, and R. Claessen, Science **357**, 287 (2017).
[35] G. Bergmann, Phys. Rep. **107**, 1 (1984).
[36] Y. Asada, K. Slevin, and T. Ohtsuki, Phys. Rev. B **70**, 035115 (2004).
[37] C. W. J. Beenakker, D. I. Pikulin, T. Hyart, H. Schomerus, and J. P. Dahlhaus, Phys. Rev. Lett. **110**, 017003 (2013).
[38] A. P. Higginbotham, S. M. Albrecht, G. Kiršanskas, W. Chang F. Kuemmeth, P. Krogstrup, T. S. Jespersen, J. Nygård, K. Flensberg, and C. M. Marcus, Nat. Phys. **11**, 1017 (2015).
[39] F. Dolcini, M. Houzet, and J. S. Meyer, Phys. Rev. B **92**, 035428 (2015).
[40] F. Chiodi, M. Ferrier, K. Tikhonov, P. Virtanen, T. Heikkilá, M. Feigelman, S. Guéron, and H. Bouchiat, Sci. Rep. **1**, 3 (2011).
[41] B. Dassonneville, M. Ferrier, S. Gueron, and H. Bouchiat, Phys. Rev. Lett. **110**, 217001 (2013).
[42] M. Ferrier, B. Dassonneville, S. Guéron, and H. Bouchiat, Phys. Rev. B **88**, 174505 (2013).
[43] C. Janvier, L. Tosi, L. Bretheau, C. Girit, M. Stern, P. Bertet, P. Joyez, D. Vion, D. Esteve, M. F. Goffman, H. Pothier, and C. Urbina, Science **349**, 1199 (2015).
[44] L. Bretheau, C. Girit, H. Pothier, D. Esteve, and C. Urbina, Nature (London) **499**, 312 (2013).
[45] D. J. van Woerkom, A. Proutski, B. van Heck, D. Bouman, J. I. Värynen, L. I. Glazman, P. Krogstrup, J. Nygård, L. P. Kouwenhoven, and A. Geresdi, arXiv:1609.00333.
[46] N. Trivedi and D. A. Browne, Phys. Rev. B **38**, 9581 (1988).
[47] S. V. Lempitsky, Sov. Phys. JETP **58**, 624 (1983).
[48] P. Virtanen, F. S. Bergeret, J. C. Cuevas, and T. T. Heikkilá, Phys. Rev. B **83**, 144514 (2011).
[49] K. S. Tikhonov and M. V. Feigelman, Phys. Rev. B **91**, 054519 (2015).
[50] D. Averin and H. T. Imam, Phys. Rev. Lett. **76**, 3814 (1996); A. Martín-Rodero, A. Levy Yeyati, and F. J. Garcia-Vidal, Phys. Rev. B **53**, R8891(R) (1996).
[51] D. Sticlet and J. Cayssol, Phys. Rev. B **90**, 201303(R) (2014).
[52] J. I. Vayrynen, G. Rastelli, W. Belzig, and L. I. Glazman, Phys. Rev. B **92**, 134508 (2015).
[53] O. Dmytruk, M. Trif, and P. Simon, Phys. Rev. B **92**, 245432 (2015); **94**, 115423 (2016).
[54] Y. Peng, F. Pientka, E. Berg, Y. Oreg, and F. Von Oppen, Phys. Rev. B **94**, 085409 (2016).